J Solid State Electrochem (2008) 12:375–385
DOI 10.1007/s10008-007-0452-8

ORIGINAL PAPER

EQCM studies on Pd–Ni alloy oxidation in basic solution

M. Grdeń · A. Czerwiński

Received: 30 December 2006 / Revised: 29 September 2007 / Accepted: 9 October 2007 / Published online: 13 November 2007

Abstract Processes of electrochemical oxidation of Pd-rich Pd–Ni alloys in basic solutions were studied with the aim of electrochemical quartz crystal microbalance. Potentials of current peaks of Ni(II)/Ni(III) redox couple are independent of alloy composition. On the other hand, Ni(II)/Ni(III) redox couples formed on Pd–Ni alloys and Ni differ in respect to the structure of involved compounds and the processes of transport of the species accompanying oxidation/reduction reaction. The process of oxidation of Pd exhibits some differences between pure Pd and Pd–Ni alloys. This concerns mainly on participation of adsorbed water/OH^- in Pd oxidation process. In the initial stages of Pd oxidation, the source of oxygen is water/OH^- from the bulk of the solution. At this stage of the process, the product of Pd oxidation could be described as $Pd(OH)_2$ or $PdOH_2O$. With further progress in oxidation process, adsorbed species, water/OH^-, start to play a decisive role. Hydrous species, i.e. $Pd(OH)_2$ or $PdOH_2O$, are also reduced in the final stages of Pd(II) reduction process.

Keywords Pd–Ni alloys · Electrochemical quartz crystal microbalance (EQCM) · Palladium oxidation

This study is dedicated to the 70th birthday of Professor Oleg Petrii.

M. Grdeń · A. Czerwiński
Department of Chemistry, Warsaw University, Pasteura 1,
02-093 Warsaw, Poland

A. Czerwiński (✉)
Industrial Chemistry Research Institute, Rydygiera 8,
01-793 Warsaw, Poland
e-mail: aczerw@chem.uw.edu.pl

Introduction

Binary metal alloy electrodes containing at least one noble metal are often studied as electrodes for, e.g. hydrogen absorption [1–4], hydrogen evolution and oxidation [5–9], electrocatalytic reactions of carbon oxides and simple organic molecules [10–15], etc. For correct evaluation of obtained data, the knowledge about the real surface area and the surface alloy composition is necessary. The latter could differ from the bulk alloy composition due to surface segregation phenomena [16, 17] or specific dissolution/oxidation of one of alloy components when the electrode is in contact with an aggressive electrolyte [1, 8, 18, 19]. Both these factors could act in opposite ways, i.e. surface segregation could enrich surface with element which is, on the other hand, specifically removed from the surface by dissolution/oxidation when the surface is in contact with aggressive solution. Thus, the factor governing composition of alloy's surface depends on the electrode environment, i.e. whether electrode is in contact with vacuum or an aggressive electrolyte. Usually, studies on alloy electrodes oxidation are focused on application of surface oxidation/reduction currents in examining of the state of the electrode surface. For binary noble metal systems forming homogeneous alloy without phase separation, only single peak of reduction of surface oxides exists. It was found that potential of surface oxide reduction peak depends linearly on alloy-surface composition [11]. This allows analysing in-situ composition of alloy's surface under conditions of uninterrupted contact of the electrode with electrolyte. The method described above was utilised in studies on electrocatalytic properties of noble metal alloy electrodes [1, 10,

12, 13, 20]. The situation is more complicated in the case of alloys with phase separation (e.g. Pt–Au [21] and Pd–Au [2]) and alloys with non-noble elements that exhibit more than one peak of reduction of surface oxides, e.g. Pd–Ni [22–24]. In this case, careful identification of each separate peak must be done before starting analysis of surface state of the electrode [21]. Less work has been done in an effort to explain mechanism of surface oxidation of alloys. Detailed analysis of this problem would help in explanation whether metals constituting alloys form mixed oxides. System that seems to be most suitable for the beginning of studies on alloy surface oxidation is the one exhibiting signals apparently originating from separate elements. One of them is Pd–Ni alloy with the shape of cyclic voltammetry (CV) curve resembling shapes of curves of both metals.

Palladium and nickel form homogeneous alloy without miscibility gap in the whole range of composition [25, 26]. Lattice constant of Pd–Ni alloy decreases with increase in Ni content [25, 27]. Pd–Ni alloy composition affects its electronic, magnetic [28–30] and elastic properties [31]. Pd–Ni alloy electrodes have been a subject of study on various processes including hydrogen absorption [22–24, 32–35], hydrogen evolution and oxidation [6, 7], methanol oxidation [36] and corrosion in acidic solutions [37]. Most of published cyclic voltammetry curves for Pd–Ni alloys recorded in basic solution could be considered as a combination of respective curves for both pure metals [22–24]. The exceptions are results shown in [38], presenting for alloy with 37 at.% Ni CV curves very similar to the curves typical for pure Ni. Preservation of current peaks characteristic for both pure elements allows studying reactions of each of elements separately and comparing them to the behaviour known for pure elements. Knowledge about electrochemical reactions of each alloy component could be then utilised in real surface area and surface composition studies. It would also help in evaluation of electrocatalytic properties of alloy's surfaces. This is especially important in the case of metal oxides which structure and composition could affect many electrocatalytical processes [39–42]. In [22, 23, 32], we presented results of electrochemical quartz crystal microbalance (EQCM) studies on electrochemical absorption of hydrogen in Pd-rich Pd–Ni alloys. We showed relation between stress induced by bulk hydrogen absorption and alloy composition [22, 32]. In [32], we also discussed differences between electrochemical properties of Ni compounds on Pd–Ni and metallic Ni electrodes. The aim of this paper is to present results of studies on processes of oxidation of surface of Pd-rich Pd–Ni alloys in basic solution under conditions of cyclic voltammetry experiments. Electrochemical quartz crystal microbalance was the tool utilised in these studies.

Experimental

Pd–Ni alloys were deposited according to the procedure described in [22, 23]; bath composition was prepared on the basis of solution described in [43]. Plating bath contained $PdCl_2$ (18 g l^{-1}), $NiSO_4 7H_2O$ (25 g l^{-1}), potassium citrate (30 g l^{-1}) and NH_3 for adjusting pH up to 8–9. Electrodeposition was carried out in three-electrode system with AgCl and Ni net as reference and counter electrodes, respectively, at room temperature without de-aeration of the solution and under controlled potential conditions. Pd–Ni alloy composition was adjusted by changing of the electrode potential in the range −29 to −324 mV vs reversible hydrogen electrode (RHE). Pd content in the bulk of the alloy was found to increase with increase in potential. Because the only purpose of alloy deposition was to prepare electrodes with known alloy composition and alloy thickness, we did not make any attempt to obtain high faradaic deposition efficiency as required for technological applications. Our experimental faradaic efficiency of alloy deposition ranged from 30 to 45%, as estimated from EQCM and separate weighing experiments. Obtained efficiencies were comparable to the ones obtained during our previous work with alloy deposited on Au wire [23] and calculated on the basis of AAS (atomic absorption spectroscopy) analysis of dissolved alloys. Thickness of alloy's layer, as estimated from efficiency calculations, was ca. 0.2 μm. In present work, alloy composition was analysed with energy-dispersive analysis of X-rays (EDAX) analyser (Röntec EDR286) coupled with scanning electron microscope (LEO 435VP). Nickel content ranged from 8 to 35 at.%. The depth of EDAX ranged from 0.5 to 0.6 μm as estimated on the basis of data for pure elements and Kanaya–Okayama equation [44]. Comparison of these values with estimated thickness of alloy layer shows that the depth of EDAX analysis covered almost full thickness of Pd–Ni layer resulting in average bulk alloy composition. This way, presented bulk alloy compositions do not include effects connected to alloy composition variation on and near the surface (surface segregation and enrichment) and on the substrate/alloy boundary (epitaxy). Substrates for deposition were 5 MHz AT-cut 14 mm diameter quartz crystals covered with Au electrodes (ITR, Poland). Microbalance used was EQCM model 234 from Institute of Physical Chemistry of the Polish Academy of Sciences, described in [45]. Microbalance was calibrated experimentally by Ag^+ deposition and Ag stripping, in the same way as used in our previous works [46, 47]. Obtained sensitivity, 10.47 ng Hz^{-1}, was well-correlated with the value obtained from Sauerbrey equation with the difference not greater than 5%. The microbalance was coupled to a frequency counter (Hewlett-Packard HP

53131A), a potentiostat (Elpan EP20A) and a generator (Elpan EG20). A personal computer via ADC/ACD converter (AMBEX LC1011, Poland) controlled the system. Due to relatively long time required for acquisition of each frequency point (several ms), work with high scan rates resulted in recording of low-resolution gravimetric curves. On the other hand, work with very low scan rates, such as few mV s^{-1} and below, would result in accumulation of hardly reducible oxide/hydroxide layer and extensive alloy dissolution. We decided to apply 25 mV s^{-1} as basic potential scan rate for further work. We did not perform any further analysis of influence of potential scan rate on processes studied.

Three-electrode system was used with saturated AgCl electrode and platinum gauze wire serving as reference and counter electrode, respectively. All potentials in the text are recalculated in respect to RHE. All solutions were prepared with Millipore® water and analytical-grade reagents. All experiments were carried out at room temperature. Solutions were deoxygenated with an argon stream (purity 5.0). During the experiments, argon atmosphere was kept over the solution surface in order to minimize solution stirring that could affect microbalance oscillations.

In one of our previous papers [48], we showed changes in the shape of steady-state cH_{abs} vs E curve induced by electrochemical treatment of noble metal alloys. These changes were accompanied by evolution of the shape of CV curves. The most striking feature was appearance of multiple slopes in phase-transition region on cH_{abs} vs E curves. For most of binary alloys, such as Pd–Ni, this part of curve is attributed to $\alpha \leftrightarrow \beta$ phase transition of absorbed hydrogen. For homogeneous system without phase separation, only one slope should be observed in this potential range without any steps or inflection points, in the same way as for p–c–T curves for gas saturation [49]. As we showed in [23] and discussed in [32], the shape of cH_{abs} vs E curves obtained for Pd–Ni alloys studied does not exhibit any effects of bulk-phase separation. One can assume that bulk behaviour of Pd–Ni alloys studied by us resembles behaviour of homogenous alloys. This, however, is only assumption and requires confirmation by other techniques, such as X-ray diffraction.

Mass changes are recalculated into mole per mass units with mass calculated from EQCM response and number of moles of electroactive species obtained from measured charge. It is known that measured mass change of the process studied could contain also contribution from side processes, such as ion adsorption, and could be affected by additional effects not related to mass change (stress-induced frequency shift). In order to stress that measured frequency changes could be affected by mentioned phenomena, term "apparent molar mass" is used for description of mass per mole ratio, in the same way as in our previous publications [22, 47].

Results and discussion

General electrochemical behavior of Pd–Ni alloys

Figure 1a shows cyclic voltammetry and gravimetric curves for Pd–Ni alloy containing 35 at.% Ni. Generally, the shapes of these curves are typical for alloys containing significant amount of Pd [22–24] and are representative for whole composition range studied. The only difference is the ratio between charges of various current peaks, as it was discussed in [32]. Similar shape of CV curves was also reported for ternary Pd–Ni-Si alloys in basic solution [50]. Current signals observed on the curve could be described as follows:

I. Oxidation of absorbed (mainly) and adsorbed hydrogen. Depending on anodic potential limit and electrode history, this peak current could also contain contribution from formation of Ni(II) compounds. Those compounds are probably $\alpha Ni(OH)_2$ transformed to $\beta Ni(OH)_2$ at more positive potentials [51–56] (see discussion in [22, 32]), although for metallic Ni electrode also NiO is suggested as one of the products [53, 57–62]. Because of this uncertainty and for the sake of clarity, these compounds are referred to as Ni(II) in further text.
II. Oxidation of alloy's surface. When compared to the respective curves obtained for pure Pd and Ni [23, 32], one could expect contribution from following processes: (a) currents of Pd oxidation to Pd(II) with the shape typical for most of noble metal electrodes (see, e.g. [18]), and (b) currents due to thickening of passive Ni (II) layer. The latter currents have a shape of featureless plateau [51, 52, 63–65] and are usually assigned to the thickening of $\beta Ni(OH)_2$ layer [66]. When CV curve starts from potentials negative enough as for significant hydrogen absorption, currents due to oxidation of absorbed hydrogen partially overlap surface currents (II) hiding onset of Pd oxidation. This is seen when Fig. 1a and b are compared; the latter one was recorded with cathodic vertex potential located before the onset of massive hydrogen absorption. Due to the fact that as proposed in the literature products of Pd oxidation to Pd (II) are both PdO as well as $Pd(OH)_2$ [39, 47, 67–71], in further text, products of Pd oxidation are labeled shortly as Pd(II).
III. Peaks of reactions of oxidation of Ni(II) (IIIa) and subsequent reduction of the oxidation products (IIIc). Usually, Bode et al. scheme [72] introduced for Ni $(OH)_2$ electrodes is utilized in analysis of these current signals. According to this model, expected Ni(II) oxidation products are various forms of NiOOH, further in the text called Ni(III). Some results, however, point

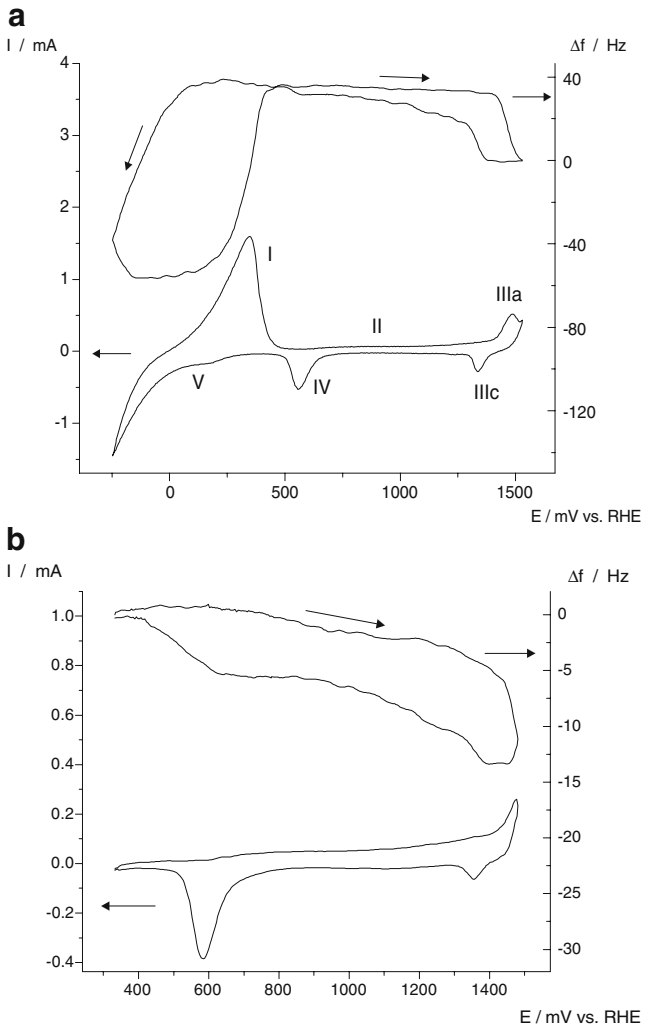

Fig. 1 Cyclic voltammetry (*lower*) and gravimetric (*upper*) curves for Pd–Ni alloy. 0.1 M KOH, 25 mV s^{-1}, room temperature. *Current peaks labeled with numbers* are described in the text. Potential range, **a** 35 at. ?% Ni, −249 to 1,530 mV; **b** 8.2 at.% Ni, −330 to 1,480 mV

out to significant differences between processes taking place on metallic Ni and $Ni(OH)_2$ electrodes [63, 73]. With further increase in anodic potential, currents due to oxygen evolution are observed.

IV. Reduction of Pd(II) compounds. This peak is often utilized for estimating of real surface area of Pd electrodes [74, 75].

V. Currents of absorption (mainly) and adsorption of hydrogen. Furthermore, depending on potential program applied and electrode history, Ni(II) reduction currents should be considered. Although these processes start already before the onset of hydrogen evolution [22, 32], at a more negative potentials, hydrogen evolution currents overlap currents (*V*).

In contrast to acidic solution [18, 46], in basic solution, gravimetric curve of Pd electrode has a shape of closed loop. Although some very slow dissolution of both metals could not be excluded, closed-frequency loop suggests that irreversible alloy dissolution during single CV scan is not a significant factor. Another factor which points on the low alloy dissolution is stability during continuous cycling of both CV and gravimetric curves. After initial CV curve evolution during first several cycles, due to ageing and surface rearrangement, stable CV curves for next few tenth cycles were observed. These curves were accompanied by stable gravimetric curves without any frequency drift that could indicate irreversible or specific alloy dissolution. This way, we can assume that in the timescale of our experiments, alloy dissolution was negligible, and dissolution phenomena do not affect Pd(II) layer formation. Since the process of hydrogen absorption in Pd–Ni alloys was the subject of our previous works [22, 23, 32], in this paper, we focus only on the processes of electrode surface oxidation. Analyzing the shape of gravimetric curves in potential region positive to peak I, the following features could be noted:

–Processes of formation and reduction of Pd(II) compounds (currents II and peak IV) are accompanied by a mass increase (frequency decrease) and a mass decrease (frequency increase), respectively. This observation agrees with the results obtained for pure Pd in various solutions [32, 47, 67, 70].

–Process of Ni(II) oxidation (peak III) is accompanied by a mass increase (frequency decrease). This effect is opposite to that observed for metallic Ni electrodes [32, 63].

Oxidation of Pd–Ni alloy surface

From CV and EQCM experiments, it is possible to draw some conclusions concerning reactions of Ni(II) compounds oxidation. Figure 2 presents the results of CV experiments with cathodic potential scan limit located positive to Pd oxide reduction region (see potential program on the inset). As an effect, during subsequent positive potential scan (procedure 2) towards Ni(II) oxidation region, electrode surface is already covered with a layer of Pd(II), and both current and mass profiles recorded for Ni(II) oxidation process are less influenced by Pd oxidation processes. This is clearly seen on gravimetric curve for anodic scan at $E>920$ mV for procedure 2. Frequency measured for procedure 2 [electrode already covered with Pd(II)] is almost constant in the same potential range where, for procedure 1, frequency decrease assigned to formation of Pd(II) was observed. Thus, reaction almost exclusively responsible for frequency decrease at $E>600$ mV is Pd

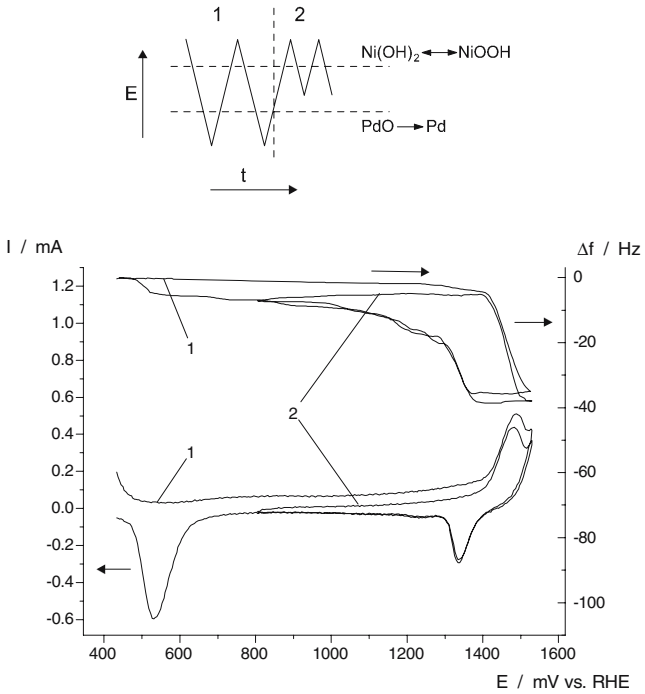

Fig. 2 Cyclic voltammetry (*lower*) and gravimetric (upper) curves for Pd–Ni alloy (35 at.% Ni) in various potential ranges according to the program shown on the *inset*. Procedure 1 includes potentials of reduction of Pd oxides, procedure 2 concerns limited potential range where only oxidation of Ni(II) and subsequent reduction of the products takes place. 0.1 M KOH, 25 mV s^{-1}

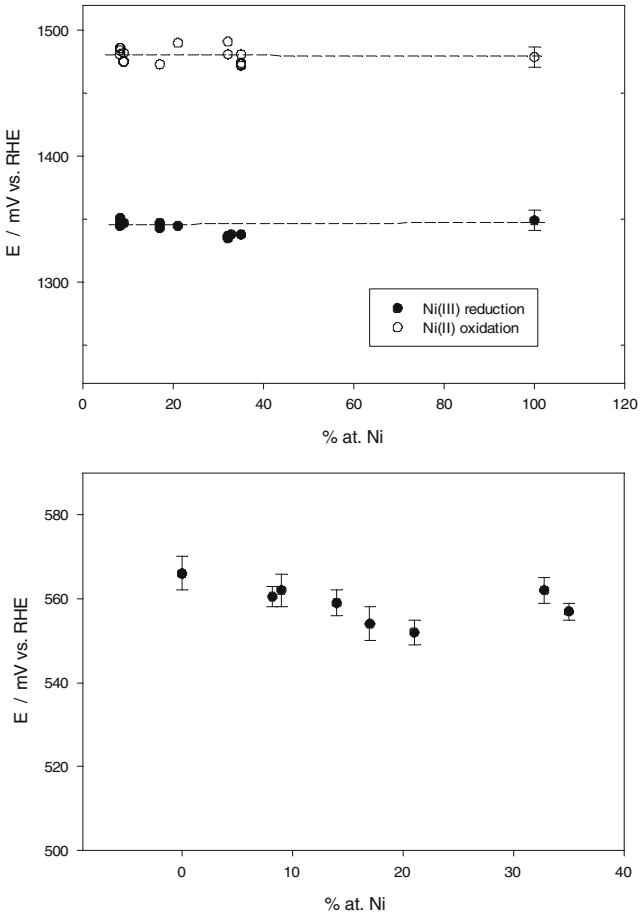

Fig. 3 Influence of alloy composition on potentials of peaks of: **a** Ni (II) oxidation and Ni(III) reduction and **b** Pd(II) reduction. 0.1 M KOH, 25 mV s^{-1}, anodic potential limit 1,530 mV

oxidation. On the other hand, for both procedures 1 and 2, frequency profile for Ni(II) oxidation and Ni(III) reduction are practically the same, undisturbed by presence of non-reduced layer of Pd(II). This way, we can conclude that the oxidation of both alloy elements proceeds independently. The fact that both elements constituting Pd–Ni alloys are oxidised separately, without formation of mixed oxides, could be understood if we consider structures of most common oxygen-containing compounds of Ni(II)/Ni(III) and Pd(II). Palladium oxide possesses tetrahedral structure [76], while the structures of $Ni(OH)_2$ and NiOOH are described as brucite-type and rhombohedral, respectively [77]. These structures differ significantly that probably prevents formation of mixed compounds.

Figure 3 presents influence of bulk alloy composition on potentials of current peaks of: (1) oxidation of Ni(II) (peak IIIa), (2) reduction of products of oxidation of Ni(II) (peak IIIc) and (3) reduction of surface Pd(II) compounds (peak IV). Anodic vertex potential was fixed at 1,530 mV. Although for pure Pd potential of Pd(II) reduction is slightly less negative than for alloys, one could note on Fig. 3b that the latter potential of this peak is almost composition-independent. For both peaks of Ni(II)/Ni(III) redox, couple peak potentials are also independent of bulk alloy composition. In [32], we reported that both qualitative as well as quantitative differences exist between oxidation of Ni(II) on metallic Ni and Pd–Ni alloy electrodes. For Pd–Ni electrodes, Ni(II) oxidation is accompanied by a mass increase (frequency decrease), while for metallic Ni, opposite effect is observed. Moreover, mass per charge ratio ("apparent molar mass") accompanying Ni(II) oxidation and reduction of Ni(III) is higher for Pd–Ni alloys and probably strongly affected by crystal lattice stresses/strains generated during the processes [32, 78]. From EQCM studies on $Ni(OH)_2$ electrodes [79–81], it is known that two main crystallographic forms of nickel hydroxide, namely $\alpha Ni(OH)_2$ and $\beta Ni(OH)_2$, exhibit different gravimetric behavior during oxidation: oxidation of the former is accompanied by a frequency decrease, while for the latter an opposite effect is observed. A comparison of data obtained for Ni and Pd–Ni electrodes presented in [32] could suggest that alloying of Ni with Pd stabilises $\alpha Ni(OH)_2$, while for metallic Ni, only frequency profile typical for $\beta Ni(OH)_2$ is observed. On the other hand, it is also known that potentials of peaks of oxidation of $\alpha Ni(OH)_2$

and $\beta Ni(OH)_2$ differ, the latter being oxidised and reduced at more positive potentials [79–81]. Thus, from the analysis of Fig. 3a and discussion presented in [32], it follows that although for Ni and Pd–Ni different mass transport occurs during Ni(II) oxidation, the thermodynamics of reactions of Ni(II)/Ni(III) is the same for both electrodes. This way, the difference between Ni and Pd–Ni electrodes seems to be limited to a transport processes accompanying Ni(II) oxidation process, i.e. transport of proton, water and/or alkali metal cations into/from the electrode. This difference between Ni and Pd–Ni alloys in respect to water/cation incorporation could result from differences in lattice constant of Ni and Pd–Ni alloys.

It is known that equilibrium composition of the surface of Pd–Ni alloys being in contact with vacuum differs from that of the bulk. Surface segregation phenomena usually lead to surface enrichment with Pd [82, 83]. In [32], we reported almost linear relation between bulk Pd–Ni alloy composition and the ratio of charges of peaks III and IV, $0.5Q_{IV}/Q_{III}$, where coefficient 0.5 is due to difference in the number of electrons exchanged in both processes. As it was discussed in [32], application of charge of peak III and Q_{IV}/Q_{III} ratio in surface composition studies is complicated. This is due to the fact that the thickness of the layer of compounds formed during oxidation of Ni(II) on metallic Ni exceeds one layer [73]. On the other hand, almost-linear relation between Q_{IV}/Q_{III} ratio and bulk alloy composition shown in [32] indicates continuous decrease in Q_{IV}/Q_{III} ratio with increase in bulk Ni content. This suggests that the changes in $0.5Q_{IV}/Q_{III}$ ratio mirror changes in surface alloy composition. If so, surface composition of alloys studied should be a linear function of bulk composition suggesting that potentials of discussed current peaks are independent of both bulk and surface alloy composition. Thus, one can conclude that analysis of redox peak potential cannot be used for in-situ estimation of surface composition of Pd–Ni alloys. More reliable data could be obtained from the analysis of charges of these peaks, as it was done in [32].

Figure 4 presents CV and gravimetric curves for Pd–Ni alloy with various anodic potential limit, E_a. Influence of E_a on potential of Pd(II) reduction peak for Pd–Ni alloys and pure Pd is shown in Fig. 5. The area of peak IV increases with the increase in E_a. This effect is initially accompanied by a positive shift in peak potential, also indicated by arrow in Fig. 4. With further increase in E_a, Pd(II) reduction peak starts to shift towards more negative values. Positive shift in Pd(II) reduction peak followed by a negative one is also observed for pure Pd electrode [84, 85]. For high enough values of E_a, another one reduction peak appears at ca. 1,000–1,200 mV, labelled in Fig. 4 as VI. This peak is also observed for pure Pd and is usually attributed to formation of Pd(IV) compounds [47, 86]. This process, however, will not be discussed in this paper.

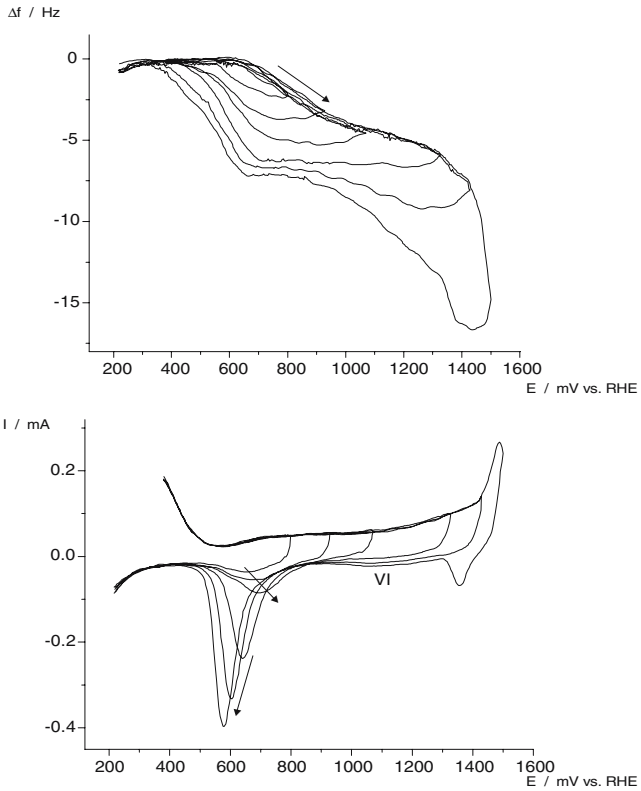

Fig. 4 Cyclic voltammetry (*lower*) and gravimetric (*upper*) curves for Pd–Ni alloy for various anodic potential limit, E_a. About 8.2 at.% Ni, 0.1 M KOH, 25 mV s^{-1}. *Arrows* indicate changes in peak potential discussed in the text

Figure 6 presents apparent molar mass changes, M_a, for Pd(II) reduction (peak IV) as a function of anodic potential limit, E_a. M_a values were calculated as a ratio $s\Delta f_{IV}/Q_{IV}$, where Δf_{IV} is the total frequency change accompanying peak IV, Q_{IV} is the charge of the peak after double-layer subtraction, and s is a coefficient containing microbalance

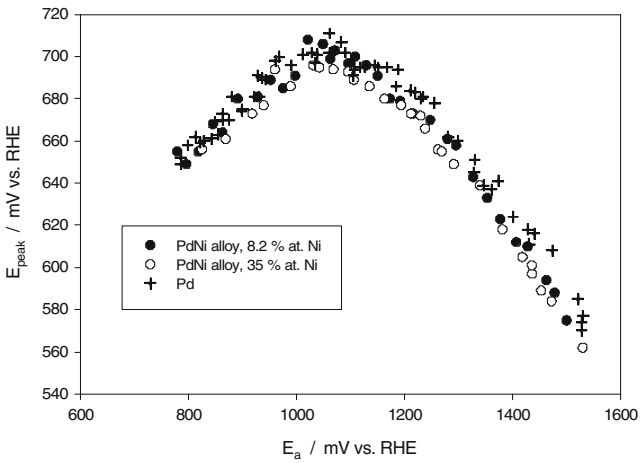

Fig. 5 Influence of anodic vertex potential, E_a, on potential of Pd(II) reduction peak for Pd–Ni alloys and pure Pd

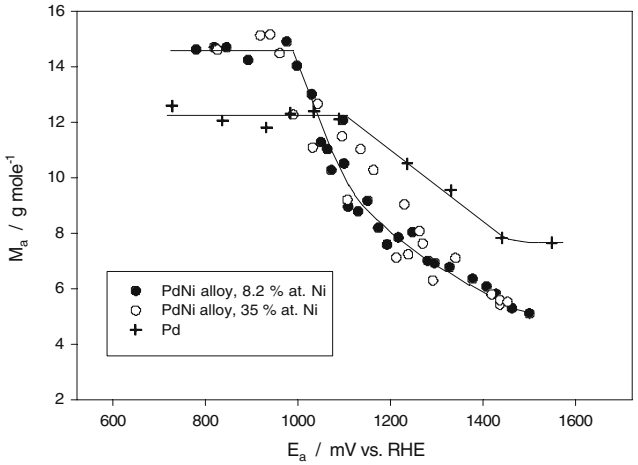

Fig. 6 Influence of anodic vertex potential, E_a, on "apparent molar mass", M_a, for Pd–Ni alloys and pure Pd

sensitivity (in mass per frequency units) and Faraday constant. According to this description, M_a value represents the effective molar mass of Pd(II) compounds being an average of M_a of all compounds constituting Pd(II) layer and reduced in potential range covering peak IV. One could note almost constant M_a value for potential below 1,000 mV for alloys and below 1,100 mV for Pd followed by a decrease in M_a with increase in anodic potential limit. In general, the shape of M_a vs E_a dependence presented on Fig. 6 for Pd–Ni alloys is very close to that found for pure Pd in basic solution [47]. The main differences between Pd and Pd–Ni electrodes are:

–Potential range where constant M_a value is observed. For metallic Pd, this region extends towards slightly more positive values than for alloys.
–Values of M_a for pure Pd and Pd–Ni differ.
–In potential range where M_a decreases with E_a, increase in the shape of M_a vs E_a dependence is linear for pure Pd while for alloys not.

Figure 7 presents Δf_{IV} vs Q_{IV} profile for Pd(II) reduction, where Δf_{IV} is frequency change and Q_{IV} is double-layer corrected-reduction charge, both recorded during CV reduction of Pd(II) compounds. These profiles were recorded for alloys with 8.2 and 35 at.% Ni and cover potential range of Pd(II) reduction peak IV. One could note two almost-linear parts of Δf_{IV} vs Q_{IV} curves labelled on the plot: I, with low slope ca. 3–4 g mole^{-1} for initial stages of the reduction process (low values of Q_{IV}), and II, covering smaller Q_{IV} range with much higher slope, ca. 12–14 g mole^{-1}. The values of these slopes are practically independent of alloy composition.

Discussion of Pd oxidation on Pd–Ni alloys

The possible reactions of Pd oxidation to Pd(II) compounds are (schematically, two-electron process):

$$Pd + OH^-/H_2O \rightarrow PdO + 2e^-; M_a = 8\ g\ mol^{-1} \quad (1a)$$

$$Pd + OH^-/H_2O \rightarrow Pd(OH)_2 + 2e^-; M_a = 17 g mol^{-1} \quad (1b)$$

$$Pd + OH^-/H_2O \rightarrow PdO\ xH_2O + 2e^-; M_a > 8 g mol^{-1} \quad (1c)$$

$$Pd + OH^-/H_2O \rightarrow Pd(OH)_2 xH_2O + 2e^-; M_a > 17 g mol^{-1} \quad (1d)$$

$$Pd + OH^-/H_2O \rightarrow xPdO + yPd(OH)_2 + 2e^-; 17 g mole^{-1} > M_a > 8 g mol^{-1} \quad (1e)$$

Presented above models include all the products reported for oxidation of Pd: PdO [47, 68–71, 87]; $Pd(OH)_2$ [39, 47, 87], hydrated Pd(II), suggested especially for thicker layers of Pd(II) [39, 67], and a mixture of PdO and $Pd(OH)_2$. These models are simplified and do not include accompanying processes, such as "place exchange" effect [88] and ion desorption. We also assume that the reduction could be considered as a process reversed to reactions [1]. Schemes presented above assume that oxygen-containing species, i.e. H_2O and/or OH^-, participating in oxidation process, originate from the bulk of the solution which results in mass gain during surface oxidation. However, it is also reasonable to assume that H_2O/OH^- present on the electrode surface already before the onset of Pd oxidation

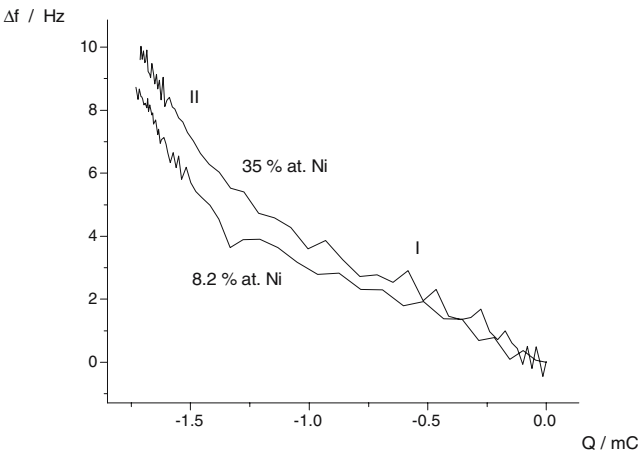

Fig. 7 Frequency change, Δf vs reduction charge, Q, profiles for reduction of Pd(II) on Pd–Ni alloys

could also participate in Pd(II) layer formation [89]. Analysing M_a vs E_a dependence presented in Fig. 6, one can assume that composition of Pd(II) layer formed in CV experiments changes with anodic potential limit. For potentials <1,000 mV, M_a values obtained for alloys are relatively close to 17 g mol^{-1}, as expected for $Pd(OH)_2$ or $PdOxH_2O$ as oxidation products. With further increase in E_a, M_a decreases, reaching values smaller than that expected for PdO, 8 g mol^{-1}.

Taking into account plot presented in Fig. 6, we can split process of Pd oxidation on Pd–Ni alloys into two steps: first one with high, almost constant value of M_a, and second one, with continuously decreasing M_a. The same scheme is applicable for Pd electrode, although both electrodes differ in respect to M_a values and its potential dependence. According to obtained M_a values, in the initial stages of Pd oxidation, structure of Pd(II) could be described as $Pd(OH)_2$ or $PdO{\cdot}xH_2O$. Mass/frequency response for both these species is the same, and it is not possible to distinguish between them using EQCM only. The same mass/frequency response is also expected for formation of $PdOH_{ads}$ adlayer, the species proposed in early models of noble metals surface oxidation [90]. However, more recent EQCM results for Pt electrode in acidic solutions [91, 92] do not confirm the idea of formation of stable layer of $M(OH)_{ads}$ species. EQCM studies on Pd electrode oxidation in acidic solution [70] also suggested formation of PdO layer only. It should be noted, however, that in [70], there are no details given about how mass changes were calculated, i.e. whether Pd active dissolution and mass/frequency changes observed at potentials negative of Pd(II) formation onset (double layer charging region) were taken into account. Significant influence of Pd dissolution on frequency response measured in acidic solution was shown and discussed in [18, 46, 87]. On the other hand, direct evidence of formation of $PdOH_{ads}$ (or more general, MOH_{ads}, for all noble metals) layer is also scarce [93] which makes assumption about formation of stable layer of $PdOH_{ads}$ in a wide potential range less probable. This way, we can assume $Pd(OH)_2$ and/or $PdO{\cdot}xH_2O$ as the most probable products formed on Pd–Ni electrode for E_a< 1,000 mV. The source of oxygen is water/OH^- from the bulk of the solution.

The decrease in M_a observed for E_a>1,000 mV is more difficult to explain. This effect could be interpreted in several ways:

–Increasing contribution from PdO species in the film formed. This assumption seems to be reasonably in the light of the results obtained with EQCM for Pt [91, 92] and Pd in acidic solutions [70]. However, resulted M_a values cannot be lower than 8 g mol^{-1}, in contrast to what is observed in Fig. 6. Formation of PdO might contribute to observed decrease in M_a, but another one process is required for explanation of the values lower than 8 g mol^{-1}. Thus, although we cannot exclude formation of PdO, furthermore, we cannot undoubtedly confirm it.

–Another one possibility is process suggested in [94, 95] leading to a mass decrease during Pd oxidation:

$$Pd + Pd(OH)_2 \rightarrow 2PdO + 2H^+ + 2e^-; M_a = -2 g mol^{-1} \quad (2)$$

However, apart from considerations presented in [94, 95], until now there is no solid evidence confirming this process. Moreover, this effect could explain only existence of parts of Δf_{IV} vs Q_{IV} plots with very low or reversed slopes (Fig. 7, reaction opposite to [2]) but cannot explain very low values of M_a obtained from the integration of whole Pd(II) reduction peak (Fig. 6). Although this mechanism is possible on the basis of analysis of Fig. 7, as it will be shown later, it cannot explain M_a values lower than 8 g mol^{-1}.

–Participation of water and/or OH^- previously adsorbed on the surface in the process of formation of Pd(II) compounds [89]. This effect is the best explanation for observed low values of M_a. Unfortunately, evaluation of water/OH^- adsorption on Pd–Ni alloys from EQCM results only is not simple. On Fig. 1b, one could note frequency almost independent of electrode potential at its values positive to Pd(II) formation onset. This effect, also reported for pure Pd, was discussed in [47, 67], where it was suggested that water/OH^- adsorption on Pd in basic solutions is insignificant or surface coverage with those species is potential-independent in this region. Intuitively, the latter sounds more convincing, but the extent of water adsorption cannot be unequivocally calculated from EQCM measurements. In [32], we presented frequency-charge profiles and M_a vs E plots for hydrogen desorption from Pd–Ni alloys. We discussed changes in the slope of frequency–charge curves for final stages of hydrogen desorption and unusual small values of M_a for some concentrations of absorbed hydrogen. We discussed adsorption of water/OH^- accompanying hydrogen desorption as one of the explanations of this effect. Although it was not possible to state unequivocally the role of adsorbed water/OH^- in this phenomenon, in the light of results discussed here, it is reasonable to assume significant water/OH^- adsorption on the alloy surface. This adsorption starts at potentials far negative of Pd(II) oxidation onset. As a result, in potential range from 330 mV to the beginning of Pd(II) formation, the surface coverage with adsorbed

species is relatively constant. Thus, the best explanation of presented results is assumption that in initial stages of Pd oxidation on Pd–Ni alloy participates mainly water/OH^- from the bulk of the solution. This results in relatively high values of M_a. With progress in oxidation process (and increase in E_a), adsorbed water/OH^- start to play decisive role in Pd oxidation. At this point, it is important to stress that from above discussion, it also follows that we cannot unequivocally confirm formation of PdO as any influence of PdO formation on M_a must overlap effects due to water/OH^- adsorption. Thus, although participation of adsorbed water/OH^- in Pd oxidation process on Pd–Ni alloys is confirmed, formation of PdO cannot be unequivocally verified. Apparently, Ni also does not contribute to frequency changes in potential range before Pd(II) formation onset. EQCM studies on pure Ni [63] show frequency changes in the same potential region, i.e. at potentials negative of Ni(II) oxidation peak, that are not observed here (see also frequency profile for procedure 2 in Fig. 2).

From Fig. 5, it follows that potential of Pd(II) reduction peak initially shifts towards more positive values and, after reaching a maximum, moves towards more negative values. Comparison of Figs. 5 and 6 indicates that mentioned maximum is close to the potential where apparent molar mass, M_a, starts to decrease from its initially high value. This way, we can link positive shift in Pd(II) reduction peak with formation of $Pd(OH)_2/PdO{\cdot}xH_2O$ species responsible for high value of M_a. Further progress in oxidation process results in decrease in M_a value, which is accompanied by a negative shift in reduction peak. More positive reduction potential indicates less stable layer of $Pd(OH)_2/PdO{\cdot}xH_2O$. It is expected that formation of a layer of noble metal oxides is accompanied by "place exchange" process resulting in formation of chessboard-like structure [68, 84, 88, 96, 97]. Progress in "place exchange" process results in increase in irreversibility of oxidation process, making reduction of generated layer more difficult, which is accompanied by a negative shift in Pd(II) reduction peak. Analysing possible Pd(II) structures, "place exchange" process seems to be more probable for PdO rather than $Pd(OH)_2/PdO{\cdot}xH_2O$. This way, negative shift in potential of peak IV could be interpreted as formation of some amounts of PdO. It should be borne in mind, however, that effects other than "place exchange" could also contribute to the shift in potential of peak IV (see, e.g. [98, 99]).

Analysis of Fig. 6 shows that high slope, close to ca. 14 g mol^{-1} is observed for initial stages of Pd(II) layer reduction. On the other hand, from Fig. 7, it follows that highest M_a value is obtained for final stages of surface oxidation, i.e. lowest E_a values in continuous CV experiments. The reason of this effect could be numerous:

–Species responsible for high values of M_a and high Δf_{IV}–Q_{IV} slope, i.e. $Pd(OH)_2$ or $PdO{\cdot}xH_2O$ are not transformed into any other form of Pd(II) compounds but even for very high values of E_a still exist on the surface being reduced at the end of Pd(II) reduction peak. This should be, however, accompanied by clear multiplicity of peak IV showing existence of two reduction peaks with different behavior in respect to increase in E_a. Reduction currents should contain: (1) preserved peak formed in the early stages of oxidation process, exhibiting positive potential shift with increase in E_a, and (2) main peak, with negative potential shift with increasing E_a (Fig. 4). This effect, however, is not observed. Moreover, positive shift in potential of reduction peak IV suggests that layer of $Pd(OH)_2/PdO{\cdot}xH_2O$ becomes more unstable with increase in E_a. This also makes less probable formation of stable layer of Pd(II) with high M_a that is reduced at the very end of reduction process.

–$Pd(OH)_2/PdO{\cdot}xH_2O$ species are transformed into less hydrous forms, e.g. in process [2]. Reaction reversed to [2] must then occur during final stages of Pd(II) reduction process. This idea could be confirmed by analysis of shape of CV curves in Fig. 4. One can note that reduction peak formed for low E_a values, for which we observe positive shift in peak potential and which could be assigned to species with high M_a, disappears or is transformed into main reduction peak with progress of oxidation process. This observation suggests that $Pd(OH)_2/PdO{\cdot}xH_2O$ species could be transformed into more anhydrous forms with the progress in surface oxidation.

–The main factor governing shape of Δf_{IV}–Q_{IV} plots observed in Fig. 7 is behaviour of oxygen-containing species released during reduction of Pd(II). Thus, species released in the early stages of reduction remain on the electrode surface adsorbed while the ones released in final stages of reduction are liberated to the solution. This implies existence on the electrode surface of active sites with different affinity towards water/OH^- adsorption. This hypothesis seems most probable on the basis of discussion of Fig. 6.

Finally, we draw some comments about differences in oxidation of Pd on pure Pd and on Pd–Ni alloys. On the basis of analysis of EQCM results for pure Pd in basic solutions, it was mentioned in [47, 67] that in "double layer charging potential region", oscillation frequency is almost constant. This effect could be interpreted as a result of lack of specific adsorption of water/OH^- or as a result of

potential independent surface coverage with adsorbed water/OH^-, with the latter possibility intuitively more probable. Bearing in mind that "apparent molar mass" obtained for later stages of Pd oxidation on Pd–Ni alloys is smaller than for Pd (descending part of M_a vs E_a curve) and that the best explanation of decrease in M_a is participation of adsorbed oxygen-containing species in Pd oxidation process, one can suggest that under the same conditions, adsorption of water/OH^- participating in Pd oxidation process is more significant on Pd–Ni alloys than on pure Pd. More detailed analysis of oxidation processes taking place on pure Pd electrode will be the subject of a subsequent communication.

Conclusions

Quartz crystal microbalance analysis of oxidation of Pd–Ni alloys in basic solutions has been performed. Pd–Ni was selected as an alloy exhibiting current signals apparently originating from each separate alloy's components. For both Pd and Pd-rich Pd–Ni alloys, "apparent molar mass" of Pd(II) compounds formed changes with anodic potential limit, although the changes are different for both electrodes. Also, mechanism of Pd(II) layer formation changes with oxidation potential. The process of Pd(II) layer formation on Pd–Ni alloys during CV scan with anodic potential limit not higher than 1,000 mV proceeds with participation of water/OH^- originating from the bulk of the solution. The structure of Pd(II) layer formed could be best described as $Pd(OH)_2$ or $PdOH_2O$. Formation of these species is accompanied by a positive shift in potential of Pd(II) reduction peak. With the increase in anodic potential limit, molar mass of Pd(II) layer decreases. This effect could be attributed to prevailing role of species, i.e. water/OH^-, adsorbed at more negative potentials in oxidation process. From EQCM data only, it is not possible to confirm directly formation of PdO structure. During Pd(II) reduction, Pd $(OH)_2$/$PdOH_2O$ species also appear during final stages of the process.

Potential of Ni(II) oxidation and reduction of subsequent compounds is independent of alloy composition. Regardless of difference in frequency profiles recorded during Ni (II) compound oxidation on metallic Ni and Pd–Ni alloys, one can assume the same thermodynamics of the process on both kinds of electrodes. The only differences lie in transport of species accompanying the process, i.e. proton, water and/or alkali metal cations. From analysis presented here, it follows that potentials of redox peaks observed on CV for Pd–Ni electrode could be hardly applied in analysis of alloy surface composition. More promising method should be the one based on analysis of the charges of those processes.

Acknowledgement This work was financially supported by 6 Framework Program, contract no. 032517, and by the Ministry of Science and Higher Education (MNiSW) as a research project.

References

1. Grdeń M, Piaścik A, Koczorowski Z, Czerwiński, A (2002) J Electroanal Chem 532:35
2. Łukaszewski M, Czerwiński, A (2003) Electrochim Acta 48:2435
3. Żurowski A, Łukaszewski M, Czerwiński, A (2006) Electrochim Acta 51:3112
4. Łukaszewski M, Czerwiński, A (2006) J Electroanal Chem 589:87
5. Bockris JO'M, Damjanovic A, Mannan RJ (1968) J Electroanal Chem 18:349
6. Akano UG, Smeltzer WW, Thompson DA, Davies JA (1990) J Electrochem Soc 137:2175
7. Krstajić NV, Burojević S, Vračar LM (2000) Int J Hydrogen Energy 25:635
8. Chun JH, Jeong SK (2003) Int J Hydrogen Energy 28:1333
9. Brooman EW, Kuhn AT (1974) J Electroanal Chem 49:325
10. Grdeń M, Paruszewska A, Czerwiński A (2001) J Electroanal Chem 502:91
11. Rand DAJ, Woods R (1972) J Electroanal Chem 36:57
12. Capon A, Parsons R (1975) J Electroanal Chem 65:285
13. Kadirgan F, Beden B, Leger JM, Lamy C (1981) J Electroanal Chem 125:89
14. Siwek H, Łukaszewski M, Czerwiński A (2004) Pol J Chem 78:1121
15. Watanabe M, Motoo S (1975) J Electroanal Chem 60:267
16. Overbury SH, Bertrand PA, Somorjai GA (1975) Chem Rev 75:547
17. Jabłoński A (1977) Adv Colloid Interface Sci 8:213
18. Łukaszewski M, Czerwiński, A (2006) J Electroanal Chem 589:38
19. Ticanelli E, Beery JG, Paffett MT, Cottesfeld S (1989) J Electroanal Chem 258:61
20. Ross PN, Kinoshita K, Scarpellino AJ, Stonehart P (1975) J Electroanal Chem 63:97
21. Kuśmierczyk K, Łukaszewski M, Rogulski Z, Siwek H, Kotowski J, Czerwiński A (2002) Pol J Chem 76:607
22. Grdeń M, Kuśmierczyk K, Czerwiński A (2002) J Solid State Electrochem 7:43
23. Grdeń M, Czerwiński A, Golimowski J, Bulska E, Krasnodębska-Ostręga B, Marassi R, Zamponi S (1999) J Electroanal Chem 460:30
24. Lee WJ, Pyun SI, Yang TH, Kim JD, Baek YH, Kim HG (1997) J Solid State Electrochem 1:120
25. Bidwell LR, Speiser R (1964) Acta Crystallogr 17:1473
26. Kondrashev YD, Tverdovskii IP, Vert ZL (1951) Dokl Akad Nauk USSR 78:729
27. Noh H, Flanagan TB, Gavra Z, Johnson JR, Reilly JJ (1991) Scr Metall Mater 25:2177
28. Lipec TV, Vert ZL, Tverdovskii IP (1969) Elektrokhimiya 5:71
29. Shelyapina MG, Fruchart D, Hlila EK, Miraglia S, dos Santos DS, Tavares SSM, Tobola J (2003) J Alloys Compd 356-357:218
30. Ikeda K (1987) J Appl Phys 62:4499
31. Özdemir Karta S, Tomak M, Çağin T (2005) Physica B 355:382
32. Grdeń M, Klimek K, Czerwiński A (2006) Electrochim Acta 51:2221
33. Rosamilia JM, Abys JA, Miller B (1991) Electrochim Acta 36:1203
34. Barton JC, Green JAS, Lewis FA (1966) Trans Faraday Soc 62:960

35. Nicolas M, Burger JP, Dumoulin L (1989) Z Phys Chem NF 163:67
36. Shobha T, Aravinda CL, Bera P, Gomathi Devi L, Mayanna SM (2003) Mater Chem Phys 80:656
37. Schlecker H, Blank P, Feller HG (1979) Z Met kd 70:638
38. Vračar LJ, Burojević S, Krstajić NV (1998) Int J Hydrogen Energy 23:1157
39. Hu CC, Wen TC (1996) Electrochim Acta 41:1505
40. Petrii OA, Smirnova NV, Aminov AY (1998) Russ J Electrochem 34:1010
41. Petrii OA (1996) Electrochim Acta 41:2307
42. Trasatti S (ed) (1980) Electrodes of conductive metallic oxides. Part A. Studies in physical and theoretical chemistry. Elsevier, Amsterdam
43. Najdeker E, Golimowski J (1991) Fresenius J Anal Chem 339:868
44. Brundle CR, Evans CA Jr, Wilson S (1992) In: Fitzpatrick LE (ed) Encyclopedia of Materials Characterization. Butterworth-Heinemann, Boston
45. Koh W, Kutner W, Jones MT, Kadish KM (1993) Electroanalysis 5:209
46. Grdeń M, Kotowski J, Czerwiński A (1999) J Solid State Electrochem 3:348
47. Grdeń M, Kotowski J, Czerwiński A (2000) J Solid State Electrochem 4:273
48. Łukaszewski M, Grdeń, M, Czerwiński A (2004) J Electroanal Chem 573:87
49. Shen CC, Lee SM, Tang JC, Perng TP (2003) J Alloys Compd 356-357:800
50. Lee JW, Pyun SI, Filipek S (2003) Electrochim Acta 48:1603
51. Hahn F, Floner D, Beden B, Lamy C (1987) Electrochim Acta 32:1631
52. de Souza LMM, Kong FP, McLarmont FR, Muller RH (1997) Electrochim Acta 42:1253
53. Medway SL, Lucas CA, Kowal A, Nichols RJ, Johnson D (2006) J Electroanal Chem 587:172
54. Seyeux A, Maurice V, Klein LH, Marcus P (2005) J Solid State Electrochem 9:337
55. Seyeux A, Maurice V, Klein LH, Marcus P (2006) J Electrochem Soc 153:B453
56. Yau SL, Fan FRF, Moffat TP, Bard AJ (1994) J Phys Chem 98:5493
57. Grdeń M, Klimek K (2005) J Electroanal Chem 581:122
58. Paik W, Szklarska-Smialowska Z (1980) Surf Sci 96:401
59. Wronkowska AA (1989) Surf Sci 214:507
60. Larramona G, Gutierrez C (1990) J Electrochem Soc 137:428
61. Visscher W, Barendrecht E (1983) Surf Sci 135:436
62. Nan J, Yang Y, Lin Z (2006) Electrochimica Acta 51:4873
63. Grdeń M, Klimek K, Czerwiński A (2004) J Solid State Electrochem 8:390
64. Dmochowska M, Czerwiński, A (1998) J Solid State Electrochem 2:16
65. Kowal A, Niewiara R, Perończyk, B, Haber J (1996) Langmuir 12:2332
66. Wolf JF, Yeh LSR, Damjanovic A (1981) Electrochim Acta 26:409
67. Birss VI, Chan M, Phan T, Vanýsek P, Zhang A (1996) J Chem Soc Faraday Trans 92:4041
68. Dall'Antonia LH, Tremiliosi-Filho G, Jerkiewicz G (2001) J Electroanal Chem 502:72
69. Zou S, Chan HYH, Williams CT, Weaver MJ (2000) Langmuir 16:754
70. Tian M, Conway BE (2005) J Electroanal Chem 581:176
71. Zhang AJ, Gaur M, Birss VI (1995) J Electroanal Chem 389: 149
72. Bode H, Dehmelt K, Witte J (1966) Electrochim Acta 11:1079
73. Zhang C, Park SM (1989) J Electrochem Soc 136:3333
74. Rand DAJ, Woods RJ (1970) J Electroanal Chem 31:29
75. Breiter MW (1977) J Electroanal Chem 81:275
76. Waser J, Levy HA, Peterson SW (1953) Acta Crystallogr 6:661
77. McEwen JS (1971) J Phys Chem 75:1782
78. Faria IC, Torresi R, Gorenstein A (1993) Electrochim Acta 38:2765
79. Wehrens-Dijksma M, Notten PHL (2006) Electrochim Acta 51:3609
80. French HM, Henderson MJ, Hillman AR, Veil E (2001) J Electroanal Chem 500:192
81. Kim MS, Kim KB (1998) J Electrochem Soc 145:507
82. Stoddart CTH, Moss RL, Pope D (1975) Surf Sci 53:241
83. Bozzolo G, Noebe RD (2003) Acta Mater 51:4395
84. Bolzán AE (1995) J Electroanal Chem 380:127
85. Hu CC, Wen TC (1995) Electrochim Acta 40:495
86. Chausse V, Regull P, Victori L (1987) J Electroanal Chem 238:115
87. Juodkazis K, Juodkazyt J, Sebeka B, Stalnionis G, Lukinskas A (2003) Russian J Electrochem 39:959
88. Jerkiewicz G (1999) In: Wieckowski A (ed) Interfacial chemistry. Theory, experiment and applications. M Dekker, New York
89. Juodkazis K, Juodkazytė, J, Juodienė T, Šukienė V, Savickaja I (2006) Electrochim Acta 51:6159
90. Angerstein-Kozlowska H, Conway BE, Sharp WBA (1973) J Electroanal Chem 43:9
91. Jerkiewicz G, Vatankhah G, Lessard J, Soriaga MP, Park YS (2004) Electrochim Acta 49:1451
92. Birss VI, Chang M, Segal J (1993) J Electroanal Chem 355:181
93. Solomun T (1987) J Electroanal Chem 217:435
94. Bagotzky VS, Tarasevich MR (1979) J Electroanal Chem 101:1
95. Gossner K, Mizera E (1981) J Electroanal Chem 125:347
96. Conway BE (1995) Prog Surf Sci 49:331
97. Seo M, Aomi M (1992) J Electrochem Soc 139:1087
98. Harrington DA (1997) J Electroanal Chem 420:101
99. Appleby AJ (1975) J Electroanal Chem 68:45